OXFORD

Cerebral Cortex, 2016, 1–10

doi: 10.1093/cercor/bhw070
Original Article

ORIGINAL ARTICLE

Multivariate Associations of Fluid Intelligence and NAA

Aki Nikolaidis[1,2], Pauline L. Baniqued[1,3,4], Michael B. Kranz[1,3], Claire J. Scavuzzo[2,5], Aron K. Barbey[1], Arthur F. Kramer[1,2,3] and Ryan J. Larsen[1]

[1]Beckman Institute for Advanced Science and Technology, [2]Neuroscience Program and, [3]Psychology Department, University of Illinois at Urbana-Champaign, Urbana, IL, USA, [4]Helen Wills Neuroscience Institute, University of California, Berkeley, Berkeley, CA, USA and [5]Psychology Department, University of Alberta, Edmonton, Alberta, Canada

Address correspondence to Aki Nikolaidis. Email: g.aki.nikolaidis@gmail.com

Abstract

Understanding the neural and metabolic correlates of fluid intelligence not only aids scientists in characterizing cognitive processes involved in intelligence, but it also offers insight into intervention methods to improve fluid intelligence. Here we use magnetic resonance spectroscopic imaging (MRSI) to measure *N*-acetyl aspartate (NAA), a biochemical marker of neural energy production and efficiency. We use principal components analysis (PCA) to examine how the distribution of NAA in the frontal and parietal lobes relates to fluid intelligence. We find that a left lateralized frontal-parietal component predicts fluid intelligence, and it does so independently of brain size, another significant predictor of fluid intelligence. These results suggest that the left motor regions play a key role in the visualization and planning necessary for spatial cognition and reasoning, and we discuss these findings in the context of the Parieto-Frontal Integration Theory of intelligence.

Key words: brain size, fluid intelligence, *Gf*, magnetic resonance spectroscopy, *N*-acetyl aspartate

Introduction

Modern life requires a wide range of cognitive abilities such as acquiring new skill sets, solving unfamiliar problems, and analyzing complex patterns of information (OECD 2001; Lingenfelter 2012). Fluid intelligence (*Gf*) is the cognitive capacity that binds these abilities together; *Gf* has been defined as the ability to adapt to new problems, discriminate relations, and reason in new circumstances in ways that do not depend heavily on prior knowledge (Cattell 1943; Salthouse et al. 2008). The importance of these abilities has motivated efforts to identify neural correlates of cognition that are sensitive to changes in brain health and function (Erickson et al. 2010; Basak et al. 2011; Vo et al. 2011; Voss et al. 2011; Oelhafen et al. 2013; Nikolaidis et al. 2014).

The neural correlates of intelligence may relate to global brain properties, such as brain size (McDaniel 2005), or to local properties, such that they are specific to certain brain regions. A wide variety of experiments have demonstrated that *Gf* is associated with a distributed network of regions in the frontal and parietal cortices, including the dorsal lateral prefrontal cortex (BA 46; DLPFC), superior parietal lobe, and supramarginal gyrus (BA 7 & 40) and associated white matter (See Jung and Haier 2007 for a review). Neural correlates specific to these regions include cortical thickness (Haier et al. 2004; Colom et al. 2007; Luders et al. 2009; Barbey et al. 2012), the degree of functional activation (Gray et al. 2003; Lee et al. 2006; Choi et al. 2008), and functional connectivity (van den Heuvel et al. 2009; Cole et al. 2012; Finn et al. 2015; see Basten et al. 2015 for a recent meta analysis of functional and structural correlates of intelligence). Regional functional activation associated with *Gf* implies that regional differences in brain activity, energy production, and metabolism may also be important for *Gf*. Neural correlates related to energy production and metabolism are available from Magnetic Resonance Spectroscopy (MRS), a noninvasive technique for measuring the concentration of metabolites in tissue.

Of the metabolites that can be detected with MRS, one of the most readily detected is *N*-acetyl aspartate (NAA; Koller et al. 1984). NAA is a neurometabolite that plays an important role in both myelination and oxidative metabolism (Baslow 2000,

2003). Because it is synthesized in the mitochondria of gray matter neurons during oxidative metabolism, NAA is considered to be a marker of metabolic efficiency (Bates et al. 1996; Ross and Sachdev 2004). Some researchers have also suggested that greater NAA may reflect higher neuronal density (Pfleiderer et al. 2004) or higher mitochondrial function (Jung, Brooks, et al. 1999). After synthesis, NAA is transported to oligodendrocytes where it is converted to a myelin precursor (Madhavarao et al. 2004); higher NAA is therefore considered a biomarker of greater white matter (WM) integrity (Bjartmar et al. 2002; Baslow 2003).

The role of NAA as a marker of brain health has been reinforced by many studies that have reported positive associations between the concentration of NAA and multiple domains of cognitive function and intelligence (Jung, Brooks, et al. 1999; Ross and Sachdev 2004; Jung and Haier 2007). In these experiments, fluid intelligence is typically measured by the Ravens Standard Progressive Matrices (RPM) or by G*f*-sensitive subtests of the Wechseler Adult Intelligence Scale (WAIS), such as matrix reasoning, block design, or picture completion (Wechsler 2008). Positive correlations between performance on these tests and NAA concentration have been found in occipital-parietal WM regions (Jung, Brooks, et al. 1999; Jung et al. 2005), frontal WM (Valenzuela et al. 2000; Ross et al. 2005), centrum semiovale WM (Charlton et al. 2007), the isthmus/splenium region of the corpus callosum (Aydin et al. 2012), and right posterior medial gray matter (Jung et al. 2009). In contrast, other studies have reported no relationship between reasoning ability and NAA concentration in parietal WM (Ferguson 2002), and occipitoparietal gray matter (Valenzuela et al. 2000; Ross et al. 2005). Moreover, Jung et al. (2005) found a negative correlation between reasoning abilities, and NAA concentration has been found in frontal WM. Taken together, these results show that despite the promise of MRS to elucidate neural correlates of intelligence, the literature exhibits some inconsistency (Patel et al. 2014). This inconsistency may be caused by a variety of factors, including methodological limitations (Patel et al. 2014).

One of the primary limitations of MRS is the low signal to noise ratio (SNR). To increase metabolite signal, scans are typically performed over large regions of the brain, thereby limiting anatomical resolution. Another strategy for improving SNR is to average multiple acquisitions. This increases the time required and limits a typical study to data from only 2 or 3 single-voxel MRS acquisitions. The resulting brain coverage is too limited to sample the distributed brain regions that have been associated with intelligence. MRS Imaging (MRSI) techniques provide more efficient sampling by simultaneously acquiring spectra from multiple voxels (Pfefferbaum et al. 1999; Ozturk et al. 2009); however, only 2 studies investigating the NAA-fluid intelligence relationship have used MRSI acquisitions (Charlton et al. 2007; Jung et al. 2009). These acquisitions consisted of single slices limited to the interior portions of the brain and did not sample the lateral gray matter (GM) regions commonly associated with intelligence (Jung and Haier 2007). These studies also did not control for variation in tissue volume fraction of GM and WM between subjects, which is important because NAA concentration is greater in GM than in WM (Wang and Li 1998).

To better characterize the relationship between G*f* and NAA, we assessed G*f* using a set of 6 fluid intelligence tasks (Salthouse 2005) in 71 young adults and used magnetic resonance spectroscopic imaging (MRSI) to collect NAA concentration. Our MRSI acquisition sampled a grid of voxels that spanned bilateral frontal and parietal cortices (See Figs 1 and 2; Jung et al. 2009), including lateral gray matter. We performed quantification of the metabolites and used high-resolution anatomical information to calculate metabolite values in a set of 22 anatomically defined regions, including both gray matter and white matter regions. We applied dimension reduction through the use of principal components analysis (PCA) on the set of 22 regions and extracted

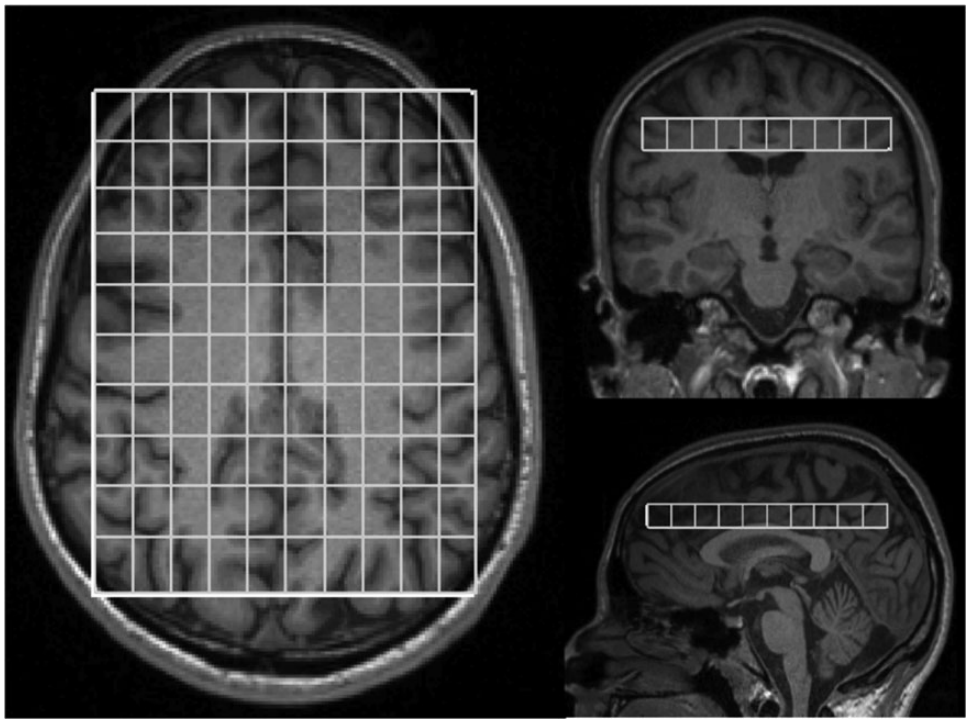

Figure 1. Representative placement of MRSI voxels relative to the MPRAGE. The 10 × 10 grid shows the voxels within the VOI where selective excitation was achieved using PRESS.

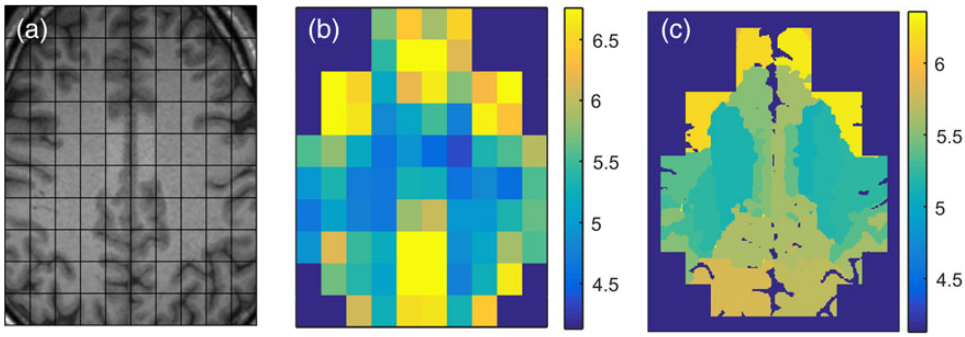

Figure 2. (*a*) Representative anatomical image of scan area. (*b*) Calculated distribution of NAA for nonexcluded voxels. (*c*) High-resolution anatomical regions are colored according to the concentration of NAA for each region.

4 components, each of which represented a set of anatomically segregated areas. We found that the Left Frontal-Parietal component, comprised the primary and premotor cortex, primary association cortex, supramarginal gyrus, and superior longitudinal fasciculus predicts *Gf* independently of brain size. These results are consistent with findings across a range of neuroimaging techniques that support the Parieto-Frontal Integration Theory (PFIT) of intelligence and demonstrate that NAA concentration in the frontal and parietal cortices relates to individual differences in intelligence.

METHODS

Participants

The University of Illinois institutional review board (IRB) approved this study. Participants were recruited from a larger pool of subjects that participated in a cognitive training study (Baniqued et al. 2014). For the cognitive training study, applicants were screened with emails and phone interviews. Eligible participants were 1) between the ages of 18 and 30, 2) devoid of major medical or psychiatric conditions, 3) right-handed, 4) devoid of non-removable metal on their body, 5) had normal or corrected-to-normal vision, and 6) reported playing video and board games for <3 h per week in the last 6 months. Of the 209 participants who completed the original training study, 74 participants received a follow-up MRSI scan. We discarded 3 of the scans due to incomplete or anomalous data for a final sample of 71 participants, 47 of whom were female. Our final sample had a mean age of 21.15 (SD = 2.566). Subjects returned for an MRSI scan an average of 154.5 days after their initial cognitive assessment performed for the cognitive training study (range: 46–456 days after). While it is not ideal that the MRSI data were collected after the intelligence tests were taken, previous work has demonstrated that such MRS estimates are stable enough to have not changed significantly in this time span (Kirov et al. 2012; Card et al. 2014).

Cognitive Tasks

Cognitive performance measures were obtained from the initial assessments of the cognitive training study (Baniqued et al. 2014). All participants performed a battery of working memory and *Gf* tasks. The *Gf* tasks' psychometric properties have been extensively investigated across a wide range of ages (Salthouse and Ferrer-Caja 2003; Salthouse 2004, 2005; Salthouse et al. 2008). The *Gf* portion of this battery is composed of 6 computerized tasks that each load highly onto a *Gf* construct. In Salthouse's structural equation model of many cognitive abilities, these 6 tasks have been grouped into 2 constructs: reasoning and spatial visualization (Salthouse 2005). The reasoning construct comprised matrix reasoning (based on the Raven's Advanced Progressive Matrices), the Shipley Abstraction task, and the Letter Sets task. The spatial visualization construct comprised the Spatial Relations task, the Paper Folding task, and the Form Boards task (See Tables 1 and 2 for a description of each task). All of the above *Gf* tasks were taken from the Virginia Cognitive Aging Project (Salthouse 2004, 2005), with the exception of the matrix reasoning task, which was modified for a functional MRI environment and is largely based on a relational reasoning task (Crone et al. 2009). To assess *Gf*, we standardized the scores from these 6 tasks and added them to create composite *Gf* scores, a simple dimension reduction technique often used with groups of collinear tasks (Valenzuela et al. 2000; Ross et al. 2005). Since these 6 tasks fall into 2 broad constructs (Salthouse 2004, 2005), we also created composite scores of spatial visualization and reasoning. To assess the specificity of the relationships to *Gf*, we also assessed working memory ability in our participants. Working memory tasks included visual short-term memory, spatial working memory, and running span (See Table 1 for descriptions of each task). It is important to note that these working memory tasks load most heavily on the short-term memory aspect of working memory, rather than the information manipulation component. We standardized the scores from these 3 tasks and added them to create composite working memory scores.

Magnetic Resonance Spectroscopy Imaging Acquisition

MRI acquisitions occurred on a Siemens (Erlangen, Germany) Trio 3T scanner with a 12-channel head coil. High-resolution anatomical information was obtained with an MPRAGE structural scan (0.9 mm isotropic, TR/TI/TE = 1900/900/2.32 ms, with GRAPPA and an acceleration factor of 2). Magnetic Resonance Spectroscopy Imaging (MRSI) was performed with a single slice 2D PRESS sequence with 16 phase encoding increments in both directions, with TR/TE = 1800/135 ms, 1 average, flip angle 90°, thickness 13 mm, weak water suppression (50 Hz BW), Hamming spatial filter of 50% width, vector size 1024, fat sat bands of thickness 30 mm, a spectral bandwidth of 2000 Hz, elliptical sampling, and acquisition time of 4′35″. The Field of View (FOV) varied with the size of the brain and was chosen to be 224 × 176, 216 × 128, 208 × 160, or 200 × 152 mm. The excitation volume, or Volume of Interest (VOI), coincided with the center 10 × 10 voxels of the 16 × 16 grid. The lower boundary of the MRSI slice was positioned transverse of the most superior portion of the corpus callosum (see Fig. 1). To minimize chemical shift error in the detection of NAA, a frequency shift of –2.7 ppm is applied, so that the region of excited NAA coincides with the designated VOI. Immediately

Table 1 Description of cognitive tasks

Gf spatial visualization	
Form Boards	Combine a set of shapes to fill a given larger shape
Paper Folding	Determine which pattern of "holes" would result from a sequence of folds followed by a punch through the paper
Spatial Relations	Analyze a 3-D figure to find the 2-D image that can be folded into the corresponding 3-D shape
Gf reasoning	
Matrix Reasoning	Find the pattern that best completes the missing cell of the matrix
Shipley Abstract	Determine how to best complete a sequence of letters and numbers
Letter sets	Assess 5 sets of letters and identify which "breaks the rule"
Working memory	
Visual Short-Term Memory	Decide whether a presented shape belonged to a previously presented set of shapes
Spatial Working Memory	Determine whether the presented dot belonged to a previous set of presented dots
Running Span	Remember the sequence of letters that is presented

Note: Scores from each task were standardized and added to create the *Gf* and working memory composite scores.

Table 2 Multiple regression results

Model	R^2	Adj. R^2	R^2 Δ	F Δ	df	Sig. F Δ
Brain size	0.165	0.151	0.165	11.662	59	0.001
Brain size, Left Frontal-Parietal NAA	0.259	0.234	0.094	7.387	58	0.009

following the first MRSI scan, a second scan with no water suppression and no frequency shift was performed to measure the water signal to aid with quantification. Eight regional saturation bands were placed on the 4 edges and 4 corners of the VOI box, perpendicular to slice direction.

MRSI voxels for which the sum of GM, WM, and cerebrospinal fluid (CSF) volume fractions is <0.995 were considered outside of the brain and marked for exclusion. Maps of tissue probability and brain regions were corrected to match the point-spread function (PSF) of the spectroscopy data by taking the Fourier transform of the structural scans and zeroing the k-space voxels that were not acquired by the MRSI scan. We also applied the same Hamming filter to the structural data that were applied to the MRSI data, before transforming the structural data back to the spatial domain. (Pfefferbaum et al. 1999; Gasparovic et al. 2006). Corrected tissue probably maps of GM, WM, and CSF were normalized at the resolution of the MRSI acquisition and used to quantify NAA concentration within each voxel (Gasparovic et al. 2006). No correction for subject motion was performed. See Supplementary Methods for details of metabolite quantification.

After quantification, we applied a cubic interpolation to the distributions of NAA concentration values to match the high resolution of the structural maps. We then integrated the interpolated distribution of metabolites over PSF-corrected maps of each of the brain regions (Fig. 2). We sampled NAA concentration from a range of cortical areas including the dorsal lateral prefrontal cortex, anterior cingulate cortex, primary motor cortex, premotor cortex, somatosensory association cortex, primary somatosensory cortex, posterior cingulate cortex, supramarginal gyrus, and inferior parietal cortex, as well as WM structures including the cingulum bundle, corpus callosum, corona radiata, and superior longitudinal fasciculus (Fig. 3). Because of the low scanning resolution inherent to our MRSI technique, each of the cortical regions sampled also included neighboring WM (see Supplementary Methods). Volume fractions of GM, WM, and CSF in each of the anatomical brain regions are obtained by integrating PSF-corrected maps of probability distribution functions over the anatomical regions.

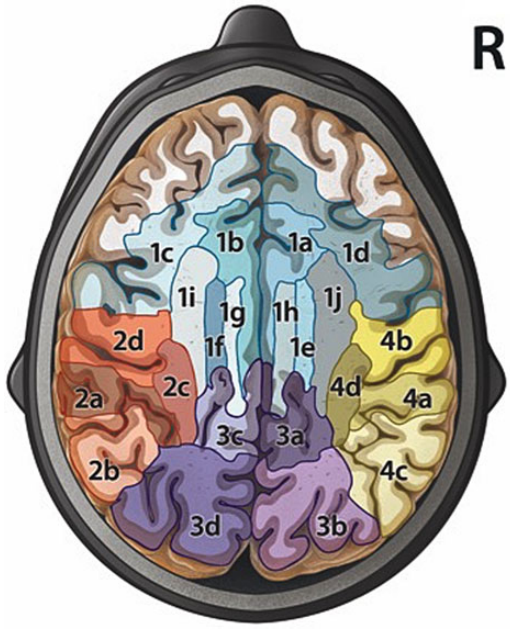

Figure 3. Representative brain regions labeled by PCA loading. This figure displays each of the sampled brain regions, color-coded by the component to which each region contributed significantly (Loading ≥0.6). The first component (Frontal; Light blue) comprised the bilateral ACC (1*a*, *b*), and the bilateral DLPFC (*c*, *d*), bilateral corpus callosum (*e*, *f*), bilateral cingulum bundle (*g*, *h*), and bilateral corona radiata (*i*, *j*). The second component (Left Frontal-Parietal; Orange) comprised the left primary somatosensory cortex (2*a*), left supramarginal gyrus (*b*), left superior longitudinal fasciculus (*c*), and left primary motor cortex and premotor cortex (*d*). The third component (Posterior Parietal; Purple) was composed of the bilateral posterior cingulate cortex (3*a*,*c*) and bilateral somatosensory association cortex (*b*, *d*), as well as the right cingulum bundle (1 h). The fourth component (Right Frontal-Parietal; Yellow) comprised the right primary somatosensory cortex (4*a*), right primary motor cortex and premotor cortex (*b*), right supramarginal gyrus (*c*), and right superior longitudinal fasciculus (*d*). The uncolored frontal regions were not acquired due to insufficient subjects with high-quality voxels in those regions.

Principal Components Analysis

To assess the distribution of NAA across the set of regions we sampled, we used PCA to organize these 22 acquired regions into a smaller set of components. NAA concentrations from all 22 bilateral cortical and WM regions, 11 per hemisphere, were entered into a PCA with varimax rotation, using Kaiser's criterion to extract components with eigenvalues larger than 1.0 (Kaiser

Table 3 Principal component analysis of regional NAA: Varimax rotated component matrix

Region	Component			
	1	2	3	4
R-ACC (1a)	**0.90**	0.18	0.19	0.08
L-ACC (1b)	**0.86**	0.28	0.21	0.22
L-DLPFC (1c)	**0.84**	0.28	0.08	0.19
R-DLPFC (1d)	**0.78**	0.15	0.02	0.38
R-Corpus Callosum (1e)	**0.72**	0.23	0.51	0.18
L-Corpus Callosum (1f)	**0.71**	0.41	0.32	0.29
L-Cingulum Bundle (1g)	**0.69**	0.39	0.48	0.22
R-Cingulum Bundle (1h)	**0.66**	0.22	**0.63**	0.11
L-Corona Radiata (1i)	**0.61**	0.54	0.21	0.33
R-Corona Radiata (1j)	**0.60**	0.26	0.41	0.47
L-Primary Som. CX (2a)	0.29	**0.84**	0.24	0.30
L-Supramarginal Gyrus (2b)	0.26	**0.82**	0.22	0.29
L-SLF (2c)	0.36	**0.80**	0.27	0.32
L-Primary Motor CX (2d)	0.51	**0.67**	0.11	0.25
R-PCC (3a)	0.24	0.22	**0.86**	0.17
R-Som. Association CX (3b)	0.10	−0.03	**0.80**	0.33
L-PCC (3c)	0.26	0.53	**0.70**	0.16
L-Som. Association CX (3d)	0.15	0.41	**0.66**	0.21
R-Primary Som. CX (4a)	0.19	0.31	0.26	**0.87**
R-Primary Motor CX (4b)	0.36	0.28	0.06	**0.82**
R-Supramarginal Gyrus (4c)	0.18	0.24	0.40	**0.78**
R-SLF (4d)	0.32	0.31	0.38	**0.75**
Eigenvector	6.53	4.29	4.17	3.89
Variance accounted for	29.70	19.49	18.93	17.68

Note: NAA regions are labeled with numbers from Figure 3. Significant contributions to a component are determined by loadings ≥0.6 and indicated by bold. Components are ordered by their eigenvectors and the percentage variance accounted for, which comprise the last 2 rows. An eigenvector can be considered the number of variables worth of data that the component represents and is directly tied to the variance accounted for, which is reported here for clarity.
DLPFC, dorsal lateral prefrontal cortex; ACC, anterior cingulate cortex; CX, cortex; PCC, posterior cingulate cortex; SLF, superior longitudinal fasciculus.

1960; Table 3). Each PCA component score is created through a weighted linear combination of NAA concentration values from each of the 22 brain regions. Regions with component loadings greater or equal to 0.6 were determined to be significant contributors to the component. We chose a varimax rotation because this extraction enforces orthogonality on the resulting components, allowing for greater ease of interpretation. To test the reliability of the components we extracted, we repeated this analysis with an oblique rotation as well and found the same set of component loadings as in the varimax rotation (see Supplementary Material). Finally, parallel analysis (PA) has been identified as a method for extracting significant components from a dataset (O'Connor 2000). By comparing each component's eigenvalue to a distribution of component eigenvalues created by permutation, this method allows for a conservative, yet nonarbitrary method for component extraction. We assessed the number of components recommended by PA as well (see Supplementary Material).

Statistical Analyses

We used 2-tailed Pearson's correlation tests to assess the relationship between our cognitive assessments and neuroimaging metrics. Each of these tests used Bias corrected accelerated 95% confidence intervals (CI) and 2000 bootstrapped samples to create a resampled range of correlation coefficients. When controlling for brain size, as well as GM and WM tissue percentage, we used 2-tailed partial correlation tests with 95% CIs and 2000 bootstrapped samples.

Results

Gf and Total Brain Size

Because *Gf* is correlated with total brain size (McDaniel 2005; Deary et al. 2010), we assessed the *Gf*–brain size relationship in our sample and found that the *Gf* composite scores demonstrate a strong correlation with brain size ($r = 0.435$, $P < 0.0001$; BCa 95% CI: $r = 0.228$:0.617; df = 68; Table 4). The effect size of this relationship is in agreement with previous literature (McDaniel 2005). We found that this relationship with brain size replicates across both spatial visualization ($r = 0.399$; $P < 0.0005$; BCa 95% CI: $r = 0.108$:0.594; df = 68), and reasoning ($r = 0.370$; $P < 0.001$; BCa 95% CI: $r = 0.169$:0.566; df = 68) subscores. When correlating spatial visualization with brain size while controlling for reasoning score, spatial visualization remained associated with brain size ($r = 0.217$; $P = 0.071$; BCa 95% CI: $r = -0.040$:0.455; df = 68); furthermore, when controlling for spatial visualization, reasoning still correlated with brain size ($r = 0.236$; $P = 0.049$; BCa 95% CI: $r = 0.012$:0.442; df = 68). These findings demonstrate that the fluid intelligence subtypes are each independently associated with brain size. Finally, we found that brain size does not predict the working memory composite score, suggesting that brain size is specifically associated with fluid intelligence (Table 4).

Distribution of NAA in the Brain

We assessed global patterns in NAA using multivariate analysis to reduce dimensionality and variance in our dataset. Toward this end, we used PCA to examine the distribution of NAA across 22 bilaterally symmetrical cortical and white mater regions in the frontal and parietal lobes. This allows us to identify groups of anatomical regions that tend to have correlated values of NAA concentration. Interestingly, the components identified by the PCA analysis comprised neighboring anatomical regions (Table 3; Fig. 3), with a clear delineation between frontal and parietal regions, as well as a separation between lateral and medial parietal regions. The first component (Frontal) comprised bilateral frontal GM regions including the anterior cingulate cortex (ACC; BA 24, 32, 33) and dorsal lateral prefrontal cortex (DLPFC; BA 9), as well as WM structures, including the bilateral corpus callosum, cingulum bundle, and corona radiata. The second component (Left Frontal-Parietal) is a left lateralized frontal-parietal component comprised the premotor and primary motor cortex (BA 4, 6), the primary somatosensory cortex (BA 1, 2, & 3), the superior longitudinal fasciculus, and the supramarginal gyrus (BA 40). The third component (Posterior Parietal) is a bilateral posterior parietal component comprised the posterior cingulate cortex (PCC; BA 23, 31), the somatosensory association cortex (BA 5, 7), and the right cingulum bundle. The fourth component (Right Frontal-Parietal) mirrors the second component but on the right hemisphere.

Regional Contributions of NAA to *Gf*

We first assessed the relationship between *Gf* and each of the components and found trending relationships between *Gf* and both the Frontal and Left Frontal-Parietal NAA components (Frontal: $r = -0.224$, $P = 0.083$, BCa 95% CI: −0.458:0.013; $n = 61$; Left Frontal-Parietal: $r = 0.218$, $P = 0.091$, BCa 95% CI: −0.067:0.501; $n = 61$). These tests do not pass corrections for multiple comparisons (Bonferroni-corrected [0.5/4] $P = 0.0125$). We also tested whether

Table 4 Correlations between Varimax NAA components, *Gf*, working memory, and brain size

Component scores	*Gf*	Working memory	Brain size
Frontal NAA	$r(61) = -0.224^{*}$ [−0.460, 0.032]	$r(61) = -0.129$ [−0.408, 0.161]	$r(61) = -0.307^{**}$ [−0.501, −0.091]
Left Frontal-Parietal NAA	$r(61) = 0.218^{*}$ [−0.067, 0.501]	$r(61) = 0.022$ [−0.214, 0.294]	$r(61) = -0.204$ [−0.454, 0.079]
Posterior-Parietal NAA	$r(61) = -0.120$ [−0.382, 0.158]	$r(61) = -0.175$ [−0.400, 0.075]	$r(61) = 0.088$ [−0.184, 0.349]
Right Frontal-Parietal NAA	$r(61) = -0.067$ [−0.399, 0.285]	$r(61) = -0.006$ [−0.265, 0.268]	$r(61) = -0.123$ [−0.366, 0.137]
Working memory	$r(71) = 0.583^{***}$ [0.422, 0.717]	—	—
Brain size	$r(71) = 0.435^{***}$ [0.228, 0.609]	$r(71) = 0.133$ [−0.082, 0.352]	—

Note: Shown are Pearson's correlations and the 95% bias-corrected and acèerated confidence intervals for bootstrapped correlations.
$^{*}P < 0.1$.
$^{**}P < 0.05$.
$^{***}P < 0.005$.

these components were associated with brain size and found that the Frontal component was significantly negatively associated with brain size, while the Left Frontal-Parietal component was negatively, but not significantly associated with brain size (Frontal: $r = -0.307$, $P = 0.016$, BCa 95% CI: −0.502:0.089; $n = 61$; Left Frontal-Parietal: $r = -0.204$, $P = 0.116$, BCa 95% CI: −0.455:0.079; $n = 61$). Both tests' 95% CI pass zero, and the Frontal component demonstrates a trending association with brain size after correcting for multiple comparisons (Bonferroni-corrected [0.5/4] $P = 0.0125$).

Given these trends, we controlled for brain size when correlating the Frontal and Left Frontal-Parietal components with *Gf*. We found that the Frontal NAA–*Gf* relationship weakened while the Left Frontal-Parietal NAA-–*Gf* relationship strengthened (Frontal: $r = -0.114$, $P = 0.384$, BCa 95% CI: −0.372:0.156; df = 58; Left Frontal-Parietal: 0.336, $P = 0.009$, BCa 95% CI: 0.079:0.562; df = 58; Bonferroni-corrected [0.5/6] $P = 0.0083$; Fig. 4), suggesting that the relationship between Frontal NAA and *Gf* is confounded by the relationship between *Gf* and brain size. We also found that Left Frontal-Parietal NAA was significantly associated with both spatial visualization ($r = 0.297$, $P = 0.021$, BCa 95% CI = 0.039:0.527) and reasoning subscores ($r = 0.289$; $P = 0.025$; BCa 95% CI = 0.045: 0.538) when controlling for brain size. To test whether either of these fluid intelligence subtypes was uniquely associated with Left Frontal-Parietal NAA, we tested the *Gf*–NAA relationship while controlling for both subtypes, and we found that the *Gf*–NAA relationship was no longer significant when controlling for either spatial visualization ($r = 0.165$; $P = 0.211$; BCa 95% CI = −0.116:0.400) or reasoning ($r = 0.178$; $P = 0.176$; BCa 95% CI = −0.075:0.414), suggesting that NAA concentration in the Left Frontal-Parietal region is generally associated with *Gf* rather than a specific subtype of *Gf*.

Previous work has demonstrated sex differences in neural correlates of intelligence (Haier et al. 2005; Jung et al. 2005). We repeated the above NAA–*Gf* correlations while controlling for gender and brain size and found these relationships unchanged (Frontal: Z = −0.011; 2-tailed $P = 0.99$; Left Frontal-Parietal: Z = −0.018; 2-tailed $P = 0.98$; Preacher 2002). Given these findings, we also assessed the *Gf* and Left Frontal-Parietal NAA relationship using a 2-step multiple regression and found both brain size and Left Frontal-Parietal NAA are each significant contributors to *Gf*, and that together they predict 25.9% of the variance in fluid intelligence (Adjusted $R^2 = 0.234$; Table 2).

Given that NAA concentration differs significantly in WM and GM, it is important to control for tissue fraction in the anatomical regions to ensure that NAA–*Gf* relationships are not driven by local differences in tissue composition. To accomplish this, we first correlated *Gf* with the NAA concentration of each region significantly contributing to the Left Frontal-Parietal component. Controlling for brain size alone, we found that the premotor and primary motor cortex ($r = 0.252$, $P = 0.036$, BCa 95% CI: 0.049:0.460; df = 68), as well as the primary somatosensory cortex were significantly associated with fluid intelligence ($r = 0.243$, $P = 0.042$, BCa 95% CI: 0.011:0.468; df = 68); whereas the supramarginal gyrus ($r = 0.164$, $P = 0.182$, BCa 95% CI: −0.085:0.413; df = 66) and superior longitudinal fasciculus were not significantly associated with *Gf* ($r = 0.176$, $P = 0.153$, BCa 95% CI: −0.059:0.396; df = 65). We then repeated the significant correlations, controlling for the volume fractions of GM and WM in each anatomical region. We found that the primary motor cortex ($r = 0.204$, $P = 0.095$, BCa 95% CI: 0.006:0.408; df = 66) as well as the primary somatosensory cortex ($r = 0.243$, $P = 0.046$, BCa 95% CI: 0.012:0.440; df = 66) display unchanged positive correlations between NAA and *Gf*. The changes in the correlation coefficient due to controlling for GM and WM are not significant (Premotor: Z = 0.273, $P = 0.785$; Primary Somatomotor: Z < 0.001, $P > 0.999$; Preacher 2002).

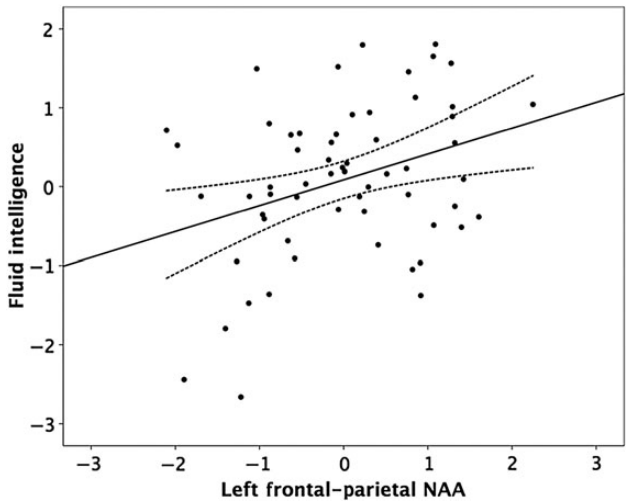

Figure 4. This scatterplot displays the distributions of the Left Frontal-Parietal NAA component and *Gf* ($R^2 = 0.114$). To visualize the relationship of NAA and *Gf* that was independent of brain size, we regressed brain size on *Gf* to calculate residuals, which represent *Gf* scores with the effect of brain size removed. These *Gf* residuals are plotted on the Y-axis. The original *Gf* scores are highly correlated with the residual *Gf* scores ($r = 0.900$; $P < 0.001$), while the residuals share no variance with brain size ($r = -0.001$; $P = 0.996$).

PA offers is a method for extracting significant components from PCA (O'Connor 2000). We performed the recommended parallel analysis using the SPSS pipeline provided by O'Connor (2000). We found that this analysis suggests we extract one rather than 4 components. Compared with our original analysis using the Kaiser Criterion (KC), PA offers a coarser breakdown of components that inhibits interpretability of our results (see

Supplementary Materials). On the other hand, both the varimax and oblique rotations of the KC PCA yield identical loadings, suggesting that while PA may be more statistically sound for extracting significant components, in this dataset it harms the interpretability of our multivariate approach.

Working Memory

Working memory ability correlated with *Gf* scores in our sample (*Gf*: $r = 0.488$, $P < 0.0001$; BCa 95% CI: $r = 0.299{:}0.650$; $n = 71$; spatial visualization: $r = 0.412$, $P < 0.0005$; BCa 95% CI: $r = 0.148{:}0.619$; $n = 71$; reasoning: $r = 0.455$, $P < 0.0001$; BCa 95% CI: $r = 0.262{:}0.638$; $n = 71$). Working memory scores were not significantly associated with brain size or with any NAA component (Table 4).

Discussion

Here we examined NAA correlates of fluid intelligence in multiple brain regions. We used a data-driven multivariate approach to assess distributions of NAA concentration across the brain and found that a group of neighboring regions in the left frontal and parietal cortices is significantly associated with *Gf*. This relationship is independent of brain size, which is also predictive of *Gf*. We then investigated NAA–*Gf* correlations within subregions of the Left Frontal-Parietal component and found that NAA concentrations in the primary motor cortex, premotor cortex, and the primary somatosensory cortex are correlated with *Gf*. While other regions, such as the prefrontal cortex, may be most commonly associated with fluid intelligence, there is a wide body of literature examining the association of the motor regions in the Left Frontal-Parietal component to spatial visualization and reasoning processes. For example, prior work has demonstrated that mathematically gifted males have been shown to activate left premotor cortex more than non-gifted males during a mental rotation task (O'Boyle et al. 2005), and lesion studies report that the left motor regions, compared with right motor regions, play a uniquely important role in critical components of spatial reasoning including both motor planning and visualization (Sabaté et al. 2004). A recent investigation of whole brain hemispheric connectivity found that high IQ participants demonstrated reduced resting state homotopic somatosensory and motor connectivity compared with average IQ individuals, providing support for the role of the left lateralized motor regions in intelligence (Santarnecchi et al. 2015). Furthermore, in a study comparing resting state to task-based functional connectivity while participants performed Raven's Progressive Matrices (RPM), researchers found that a left motor network's intrinsic coherence was significantly greater during RPM than rest (Vakhtin et al. 2014). The current results, taken together with these findings, suggest that the left motor regions are not only associated with *Gf* due to greater motor processing during on-task demands, but rather these regions play a key role in the motor visualization and planning necessary for spatial cognition and reasoning. Our results extend prior work by suggesting that in addition to activation and functional connectivity, the metabolic and white matter health of these regions may form a complex multimodal phenotype of higher fluid intelligence.

The current results suggest that Left Frontal-Parietal energy production and WM integrity, as measured by NAA, support fluid intelligence. This finding is partially consistent with the PFIT, which proposes that interactions within a distributed network of regions in the frontal and parietal cortices support intelligence (Jung and Haier 2007). This theory is formed through the convergence of a wide body of evidence from positron emission tomography (PET), functional magnetic resonance imaging (fMRI), structural MRI, and MRS. Of the 5 Brodmann's areas in the PFIT model that were at least in part included in the current study (BA 6, 7, 9, 32, and 40), we find support for 2 of these regions' association with intelligence (BA 6 & 40). When looking across all neuroimaging techniques discussed in PFIT, results demonstrate left lateralized relationships with IQ for BA 40 and bilateral relationships for BA 6, which is partially supported by the current results.

The PFIT proposes a 4-stage information processing model of intelligence (Colom et al. 2009). In the first stage, temporal and occipital regions play a role in sensory information processing, and in the second stage, parietal areas such as BA 40 are involved in integration and abstraction of this information. In the third stage, the parietal and frontal regions, including BA 6, interact to evaluate hypotheses, and in the fourth stage the ACC is involved in response selection and inhibition. In our study, the Left Frontal-Parietal component comprised 2 regions from this processing model, BA 6 and 40. Our finding that a linear combination of NAA concentration in this area predicts fluid intelligence supports the PFIT information processing theory. Specifically, these results suggest that within the Left Frontal-Parietal region, NAA, an indicator of energy production and efficiency, may be important for abstraction and integration during the second stage, as well as for hypothesis evaluation that occurs during Stage 3 of the PFIT 4-stage model of intelligence.

The fact that working memory shares more variance with *Gf* than any other cognitive domain has led some to suggest that working memory capacity and *Gf* are identical constructs (Conway et al. 2002, 2003; Engle 2002; Kane and Engle 2002; Kyllonen 2002). However, these claims have been softened due the emergence of a more detailed understanding of the processes underlying working memory (Conway et al. 2003; Kane et al. 2005). The close relationship between working memory and *Gf* may arise from the fact that they are supported by similar regions of the brain, including the superior parietal lobule and DLPFC (Cohen et al. 1997; Henson et al. 2000; Kane and Engle 2002; Pessoa et al. 2002; Todd and Marois 2005; Dahlin et al. 2008; Colom et al. 2009; Koenigs et al. 2009; Barbey et al. 2013). These regions were included in our MRSI data; however, none of our NAA components were significantly related to the measures we used to assess working memory ability. The present results imply that NAA may be sensitive to cognitive processes that are specific to fluid intelligence, not working memory. More specifically, in the context of the PFIT information processing model, our results suggest that NAA in this region may be more closely tied to the second and third stages of information processing, where fluid cognition plays a role in integrating and evaluating information to form hypotheses, as opposed to working memory-related processes such as information intake and storage, which occurs in the first processing stage. In this way, Left Frontal-Parietal NAA may support reasoning and spatial visualization, but not working memory or processes closely related to short-term memory. However, future studies should attempt to replicate and explore these relationships further, perhaps using working memory tests that are less short-term memory focused and more sensitive individual differences in young adults, given the fact that studies in children have found correlations between working memory and NAA (Yeo et al. 2000; Ozturk et al. 2009).

Brain size is also specifically predictive of intelligence and not working memory. Our finding that the NAA and brain size relationship is independent of the NAA–*Gf* relationship suggests that brain size and NAA may affect *Gf* via separate mechanisms. Total size is a genetically determined global structural property

of the brain (Tramo et al. 1998). In contrast, NAA concentration is a local metabolic property, and it may be more susceptible to environmental factors such as diet or fitness (Erickson et al. 2012). Regional NAA distributions may therefore serve as a biomarker of *Gf* that may be modified through interventions.

Mapping the distribution of NAA in the brain is an important step towards appreciating its function in cognitive processes. Although previous research has assessed the distribution of NAA in the rodent and human central nervous system (Koller et al. 1984; Soher et al. 1996; Maudsley et al. 2009) to the best of our knowledge, this is the first study to use data-driven multivariate methods to describe distributions of NAA in humans. The current work implies that the distribution of NAA follows roughly anatomical divisions, with gross distinctions between the frontal and parietal lobes, as well as segregations between medial and lateral parietal regions. However, these results should be interpreted with caution, because it is expected that neighboring regions will share some variance because of the low sampling resolution, which causes the point spread function of the acquisition to smooth the NAA signal into neighboring regions. To reduce this effect, experiments at higher resolution are required. Despite the possibility that our results are influenced by the point spread function, the consistency of NAA concentration across neighboring anatomical regions suggests that data-driven techniques are effective for dimension reduction of spectroscopy data. Furthermore, a limitation of the current work is that the MRSI data were collected a significant period of time after the intelligence tests were taken. While this is not ideal, previous work suggests that such MRS estimates are stable enough to have not changed significantly in this time (Kirov et al. 2012; Card et al. 2014).

The PCA analysis performed here can also be used to determine whether other metabolites exhibit similar groupings between anatomical regions. A variety of studies have probed relationships between intelligence and other metabolites measured by MRS, such as total creatine signal and total choline signal (Ross and Sachdev 2004). This literature exhibits a variety of inconsistent results related to the direction and strength of these correlations (Buckley et al. 1994; Jung, Yeo, et al. 1999; Ferguson 2002; Aydin et al. 2012). Further work is needed to confirm whether these metabolites relate to intelligence.

Future studies should make use of MRSI pulse sequences that allow full brain coverage within reasonable scan times. Because these sequences can rapidly acquire data, they are capable of achieving higher resolution data, which is critical for achieving better coverage of lateral cortical regions (Lam and Liang 2014; Lecocq et al. 2014). This information will facilitate the interpretation of results by allowing more fine-grained distinctions to be made between white matter and gray matter contributions to NAA concentration values. Finally, NAA is reflective of myelin health (Baslow 2003); therefore, it is of particular interest to pair a high-resolution spectroscopy acquisition with diffusion-weighted imaging such as diffusion tensor imaging (DTI) or diffusion spectrum imaging (DSI) to investigate the relationships between fractional anisotropy, NAA, and *Gf*. This extends to other neuroimaging modalities as well; understanding how individual differences in NAA are tied to variation in other neuroimaging metrics such as functional connectivity would offer a clearer understanding of the role NAA plays in cognition and brain function.

Conclusions

We find that Left Frontal-Parietal NAA, a biomarker of brain health and metabolism, predicts *Gf* independently of variation in global and regional brain structure. These results are consistent with the Parieto-Frontal Integration Theory of intelligence and demonstrate the importance of brain metabolism in higher order cognitive processing. Given NAA's purported role as an intervention biomarker, this imaging modality may see beneficial application in assessing effects of interventions aimed at improving intelligence.

Supplementary Material

Supplementary material can be found at: http://www.cercor.oxfordjournals.org/.

Funding

This work was supported by the Office of Naval Research (grant no. N000140710903 to A.F.K.), Abbott Nutrition through the Center for Nutrition, Learning, and Memory at the University of Illinois at Urbana-Champaign (grant ANGC1209 to R.J.L.), and National Science Foundation (Graduate Research Fellowship to A.N., and grant no. 0903622 to P.L.B.).

Notes

We thank Zhi-Pei Liang, Brad Sutton, Tracey Wszalek for technical guidance, and Michael Newman for assistance with data processing. We thank Nancy Dodge, Holly Tracy, Grace Song, and members of the Lifelong Brain and Cognition Laboratory for assistance with performing the experiments. *Conflict of Interest*: None declared.

References

Aydin K, Uysal S, Yakut A, Emiroglu B, Yilmaz F. 2012. N-acetylaspartate concentration in corpus callosum is positively correlated with intelligence in adolescents. Neuroimage. 59:1058–1064.

Baniqued PL, Kranz MB, Voss MW, Lee H, Cosman JD, Severson J, Kramer AF. 2014. Cognitive training with casual video games: points to consider. Front Psychol. 4:1–19.

Barbey AK, Colom R, Paul EJ, Grafman J. 2013. Architecture of fluid intelligence and working memory revealed by lesion mapping. Brain Struct Funct. 219:485–494.

Barbey AK, Colom R, Solomon J, Krueger F, Forbes C, Grafman J. 2012. An integrative architecture for general intelligence and executive function revealed by lesion mapping. Brain. 135:1154–1164.

Basak C, Voss MW, Erickson KI, Boot WR, Kramer AF. 2011. Regional differences in brain volume predict the acquisition of skill in a complex real-time strategy videogame. Brain Cogn. 76:407–414.

Baslow MH. 2000. Functions of N-acetyl-L-aspartate and N-acetyl-L-aspartylglutamate in the vertebrate brain: role in glial cell-specific signaling. J Neurochem. 75:453–459.

Baslow MH. 2003. N-acetylaspartate in the vertebrate brain: metabolism and function. Neurochem Res. 28:941–953.

Basten U, Hilger K, Fiebach CJ. 2015. Where smart brains are different: a quantitative meta-analysis of functional and structural brain imaging studies on intelligence. Intelligence. 51:10–27.

Bates TE, Strangward M, Keelan J, Davey GP, Munro PM, Clark JB. 1996. Inhibition of N-acetylaspartate production: implications for 1H MRS studies in vivo. Neuroreport. 7:1397–1400.

Bjartmar C, Battistuta J, Terada N, Dupree E, Trapp BD. 2002. N-acetylaspartate is an axon-specific marker of mature white matter in vivo: a biochemical and immunohistochemical study on the rat optic nerve. Ann Neurol. 51:51–58.

Buckley PF, Moore C, Long H, Larkin C, Thompson P, Mulvany F, Redmond O, Stack JP, Ennis JT, Waddington JL. 1994. 1H-magnetic resonance spectroscopy of the left temporal and frontal lobes in schizophrenia: clinical, neurodevelopmental, and cognitive correlates. Biol Psychiatry. 36:792–800.

Card D, Taylor MJ, Sled JG. 2014. MRS in development and across the life span. In: Magnetic Resonance Spectroscopy. Amsterdam: Elsevier Inc. p. 254–265.

Cattell RB. 1943. The measurement of adult inteligence. Psychol Bull. 40:153–193.

Charlton RA, McIntyre DJO, Howe FA, Morris RG, Markus HS. 2007. The relationship between white matter brain metabolites and cognition in normal aging: the GENIE study. Brain Res. 1164:108–116.

Choi YY, Shamosh NA, Cho SH, DeYoung CG, Lee MJ, Lee J-M, Kim SI, Cho Z-H, Kim K, Gray JR, et al. 2008. Multiple bases of human intelligence revealed by cortical thickness and neural activation. J Neurosci. 28:10323–10329.

Cohen JD, Perlstein W, Braver T, Nystrom L, Noll DC, Jonides J, Smith EE. 1997. Temporal dynamics of brain activation during a working memory task. Nature. 386:604–608.

Cole MW, Yarkoni T, Repovs G, Anticevic A, Braver TS. 2012. Global connectivity of prefrontal cortex predicts cognitive control and intelligence. J Neurosci. 32:8988–8999.

Colom R, Haier RJ, Head K, Álvarez-Linera J, Quiroga MÁ, Shih PC, Jung RE. 2009. Gray matter correlates of fluid, crystallized, and spatial intelligence: testing the P-FIT model. Intelligence. 37:124–135.

Colom R, Jung RE, Haier RJ. 2007. General intelligence and memory span: evidence for a common neuroanatomic framework. Cogn Neuropsychol. 24:867–878.

Conway ARA, Cowan N, Bunting MF, Therriault DJ, Minkoff SRB. 2002. A latent variable analysis of working memory capacity, short-term memory capacity, processing speed, and general fluid intelligence. Intelligence. 30:163–183.

Conway ARA, Kane MJ, Engle RW. 2003. Working memory capacity and its relation to general intelligence. Trends Cogn Sci. 7:547–552.

Crone EA, Wendelken C, Van Leijenhorst L, Honomichl RD, Christoff K, Bunge SA. 2009. Neurocognitive development of relational reasoning. Dev Sci. 12:55–66.

Dahlin E, Neely AS, Larsson A, Bäckman L, Nyberg L. 2008. Transfer of learning after updating training mediated by the striatum. Science. 320:1510–1512.

Deary IJ, Penke L, Johnson W. 2010. The neuroscience of human intelligence differences. Nat Rev Neurosci. 11:201–211.

Engle RW. 2002. Working memory capacity as executive attention. Curr Dir Psychol Sci. 11:19.

Erickson KI, Boot WR, Basak C, Neider MB, Prakash RS, Voss MW, Graybiel AM, Simons DJ, Fabiani M, Gratton G, et al. 2010. Striatal volume predicts level of video game skill acquisition. Cereb Cortex. 20:2522–2530.

Erickson KI, Weinstein AM, Sutton BP, Prakash RS, Voss MW, Chaddock L, Szabo AN, Mailey EL, White SM, Wojcicki TR, et al. 2012. Beyond vascularization: aerobic fitness is associated with N-acetylaspartate and working memory. Brain Behav. 2:32–41.

Ferguson KJ. 2002. Magnetic resonance spectroscopy and cognitive function in healthy elderly men. Brain. 125: 2743–2749.

Finn ES, Shen X, Scheinost D, Rosenberg MD, Huang J, Chun MM, Papademetris X, Constable RT. 2015. Functional connectome fingerprinting: identifying individuals using patterns of brain connectivity. Nat Neurosci. 18:1664–1671.

Gasparovic C, Song T, Devier D, Bockholt HJ, Caprihan A, Mullins PG, Posse S, Jung RE, Morrison LA. 2006. Use of tissue water as a concentration reference for proton spectroscopic imaging. Magn Reson Med. 55:1219–1226.

Gray JR, Chabris CF, Braver TS. 2003. Neural mechanisms of general fluid intelligence. Nat Neurosci. 6:316–322.

Haier RJ, Jung RE, Yeo RA, Head K, Alkire MT. 2005. The neuroanatomy of general intelligence: sex matters. Neuroimage. 25:320–327.

Haier RJ, Jung RE, Yeo RA, Head K, Alkire MT. 2004. Structural brain variation and general intelligence. Neuroimage. 23:425–433.

Henson RNA, Burgess N, Frith CD. 2000. Recoding, storage, rehearsal and grouping in verbal short-term memory: an fMRI study. Neuropsychologia. 38:426–440.

Jung RE, Brooks WM, Yeo RA, Chiulli SJ, Weers DC, Sibbitt WL. 1999. Biochemical markers of intelligence: a proton MR spectroscopy study of normal human brain. Proc Biol Sci. 266:1375–1379.

Jung RE, Gasparovic C, Chavez RS, Caprihan A, Barrow R, Yeo RA. 2009. Imaging intelligence with proton magnetic resonance spectroscopy. Intelligence. 37:192–198.

Jung RE, Haier RJ. 2007. The Parieto-Frontal Integration Theory (P-FIT) of intelligence: converging neuroimaging evidence. Behav Brain Sci. 30:135–154; discussion 154–187.

Jung RE, Haier RJ, Yeo RA, Rowland LM, Petropoulos H, Levine AS, Sibbitt WL, Brooks WM. 2005. Sex differences in N-acetylaspartate correlates of general intelligence: an 1H-MRS study of normal human brain. Neuroimage. 26:965–972.

Jung RE, Yeo RA, Chiulli SJ, Sibbitt WL, Weers DC, Hart BL, Brooks WM. 1999. Biochemical markers of cognition: a proton MR spectroscopy study of normal human brain. Neuroreport. 10:3327–3331.

Kaiser HF. 1960. The application of electronic computers to factor analysis. Educ Psychol Meas. 20:141–151.

Kane MJ, Engle RW. 2002. The role of prefrontal cortex in working-memory capacity, executive attention, and general fluid intelligence: an individual-differences perspective. Psychon Bull Rev. 9:637–671.

Kane MJ, Hambrick DZ, Conway ARA. 2005. Working memory capacity and fluid intelligence are strongly related constructs: comment on Ackerman, Beier, and Boyle (2005). Psychol Bull. 131:66–71; author reply 72–75.

Kirov II, George IC, Jayawickrama N, Babb JS, Perry NN, Gonen O. 2012. Longitudinal inter- and intra-individual human brain metabolic quantification over 3 years with proton MR spectroscopy at 3T. Magn Reson Med. 67:27–33.

Koenigs M, Barbey AK, Postle BR, Grafman J. 2009. Superior parietal cortex is critical for the manipulation of information in working memory. J Neurosci. 29:14980–14986.

Koller KJ, Zaczek R, Coyle JT. 1984. N-acetyl-aspartyl-glutamate: regional levels in rat brain and the effects of brain lesions as determined by a new HPLC method. J Neurochem. 43:1136–1142.

Kyllonen P. 2002. g: Knowledge, speed, strategies, or working-memory capacity? In: Sternberg RJ, Grigorenko EL, editors. The general factor of intelligence: how general is it. Hove, UK: Psychology Press. p. 415–445.

Lam F, Liang ZP. 2014. A subspace approach to high-resolution spectroscopic imaging. Magn Reson Med. 71:1349–1357.

Lecocq A, Le Fur Y, Maudsley AA, Le Troter A, Sheriff S, Sabati M, Donnadieu M, Confort-Gouny S, Cozzone PJ, Guye M, et al. 2014. Whole-brain quantitative mapping of metabolites using short echo three-dimensional proton MRSI. J Magn Reson Imaging. 42(2):280–289.

Lee KH, Choi YY, Gray JR, Cho SH, Chae J-H, Lee S, Kim K. 2006. Neural correlates of superior intelligence: stronger recruitment of posterior parietal cortex. Neuroimage. 29:578–586.
Lingenfelter PE. 2012. The Knowledge Economy: Challenges and Opportunities for American Higher Education. In Oblinger DG, editor. Game Changers: Education and Information Technologies. Louisville: EDUCAUSE. p. 9–23
Luders E, Narr KL, Thompson PM, Toga AW. 2009. Neuroanatomical correlates of intelligence. Intelligence. 37:156–163.
Madhavarao CN, Moffett JR, Moore RA, Viola RE, Namboodiri MAA, Jacobowitz DM. 2004. Immunohistochemical localization of aspartoacylase in the rat central nervous system. J Comp Neurol. 472:318–329.
Maudsley AA, Domenig C, Govind V, Darkazanli A, Studholme C, Arheart K, Bloomer C. 2009. Mapping of brain metabolite distributions by volumetric proton MR spectroscopic imaging (MRSI). Magn Reson Med. 61:548–559.
Mcdaniel M. 2005. Big-brained people are smarter: a meta-analysis of the relationship between in vivo brain volume and intelligence. Intelligence. 33:337–346.
Nikolaidis A, Voss MW, Lee H, Vo LTK, Kramer AF. 2014. Parietal plasticity after training with a complex video game is associated with individual differences in improvements in an untrained working memory task. Front Hum Neurosci. 8:1–11.
O'Boyle MW, Cunnington R, Silk TJ, Vaughan D, Jackson G, Syngeniotis A, Egan GF. 2005. Mathematically gifted male adolescents activate a unique brain network during mental rotation. Cogn Brain Res. 25:583–587.
O'Connor BP. 2000. SPSS and SAS programs for determining the number of components using parallel analysis and velicer's MAP test. Behav Res Methods Instrum Comput. 32:396–402.
OECD. 2001. Competencies for the knowledge economy. Retrieved from http://www.oecd.org/innovation/research/1842070.pdf.
Oelhafen S, Nikolaidis A, Padovani T, Blaser D, Koenig T, Perrig WJ. 2013. Increased parietal activity after training of interference control. Neuropsychologia. 51:2781–2790.
Ozturk A, Degaonkar M, Matson MA, Wells CT, Mahone EM, Horská A. 2009. Proton MR spectroscopy correlates of frontal lobe function in healthy children. AJNR Am J Neuroradiol. 30:1308–1314.
Patel T, Blyth JC, Griffiths G, Kelly D, Talcott JB. 2014. Moderate relationships between NAA and cognitive ability in healthy adults: implications for cognitive spectroscopy. Front Hum Neurosci. 8:39.
Pessoa L, Gutierrez E, Bandettini PA, Ungerleider LG. 2002. Neural correlates of visual working memory. Neuron. 35:975–987.
Pfefferbaum A, Adalsteinsson E, Spielman D, Sullivan EV, Lim KO. 1999. In vivo spectroscopic quantification of the N-acetyl moiety, creatine, and choline from large volumes of brain gray and white matter: Effects of normal aging. Magn Reson Med. 41:276–284.
Pfleiderer B, Ohrmann P, Suslow T, Wolgast M, Gerlach AL, Heindel W, Michael N. 2004. N-acetylaspartate levels of left frontal cortex are associated with verbal intelligence in women but not in men: a proton magnetic resonance spectroscopy study. Neuroscience. 123:1053–1058.
Preacher KJ. 2002. Calculation for the test of the difference between two independent correlation coefficients. Available from: URL http//quantpsy.org, last accessed 15 December 2015.
Ross AJ, Sachdev PS. 2004. Magnetic resonance spectroscopy in cognitive research. Brain Res Brain Res Rev. 44:83–102.
Ross AJ, Sachdev PS, Wen W, Valenzuela MJ, Brodaty H. 2005. Cognitive correlates of 1H MRS measures in the healthy elderly brain. Brain Res Bull. 66:9–16.
Sabaté M, González B, Rodríguez M. 2004. Brain lateralization of motor imagery: motor planning asymmetry as a cause of movement lateralization. Neuropsychologia. 42:1041–1049.
Salthouse TA. 2004. Localizing age-related individual differences in a hierarchical structure. Intelligence. 32:541–561.
Salthouse TA. 2005. Relations between cognitive abilities and measures of executive functioning. Neuropsychology. 19:532–545.
Salthouse TA, Ferrer-Caja E. 2003. What needs to be explained to account for age-related effects on multiple cognitive variables? Psychol Aging. 18:91–110.
Salthouse TA, Pink JE, Tucker-Drob EM. 2008. Contextual analysis of fluid intelligence. Intelligence. 36:464–486.
Santarnecchi E, Tatti E, Rossi S, Serino V, Rossi A. 2015. Intelligence-related differences in the asymmetry of spontaneous cerebral activity. Hum Brain Mapp. 36:3586–3602.
Soher BJ, van Zijl PC, Duyn JH, Barker PB. 1996. Quantitative proton MR spectroscopic imaging of the human brain. Magn Reson Med. 35:356–363.
Todd JJ, Marois R. 2005. Posterior parietal cortex activity predicts individual differences in visual short-term memory capacity. Cogn Affect Behav Neurosci. 5:144–155.
Tramo MJ, Loftus WC, Stukel TA, Green RL, Weaver JB, Gazzaniga MS. 1998. Brain size, head size, and intelligence quotient in monozygotic twins. Neurology. 50:1246–1252.
Vakhtin AA, Ryman SG, Flores RA, Jung RE. 2014. Functional brain networks contributing to the Parieto-Frontal Integration Theory of Intelligence. Neuroimage. 103:349–354.
Valenzuela MJ, Sachdev PS, Wen W, Shnier R, Brodaty H, Gillies D. 2000. Dual voxel proton magnetic resonance spectroscopy in the healthy elderly: subcortical-frontal axonal N-acetylaspartate levels are correlated with fluid cognitive abilities independent of structural brain changes. Neuroimage. 12:747–756.
van den Heuvel MP, Stam CJ, Kahn RS, Hulshoff Pol HE. 2009. Efficiency of functional brain networks and intellectual performance. J Neurosci. 29:7619–7624.
Vo LTK, Walther DB, Kramer AF, Erickson KI, Boot WR, Voss MW, Prakash RS, Lee H, Fabiani M, Gratton G, et al. 2011. Predicting individuals' learning success from patterns of pre-learning MRI activity. PLoS One. 6:e16093.
Voss MW, Prakash RS, Erickson KI, Boot WR, Basak C, Neider MB, Simons DJ, Fabiani M, Gratton G, Kramer AF. 2011. Effects of training strategies implemented in a complex videogame on functional connectivity of attentional networks. Neuroimage. 59(1):138–148.
Wang Y, Li SJ. 1998. Differentiation of metabolic concentrations between gray matter and white matter of human brain by in vivo 1H magnetic resonance spectroscopy. Magn Reson Med. 39:28–33.
Wechsler D. 2008. Wechsler adult intelligence scale–fourth edition (WAIS–IV). San Antonio (TX): NCS Pearson.
Yeo RA, Hill D, Campbell R, Vigil J, Brooks WM. 2000. Developmental instability and working memory ability in children: a magnetic resonance spectroscopy investigation. Dev Neuropsychol. 17:143–159.